Bone 120 (2019) 219–231

Contents lists available at ScienceDirect

Bone

journal homepage: www.elsevier.com/locate/bone

Full Length Article

Mouse polycomb group gene *Cbx2* promotes osteoblastic but suppresses adipogenic differentiation in postnatal long bones

Yuko Katoh-Fukui[a,*], Takashi Baba[b,c], Tetsuya Sato[c,d,e], Hiroyuki Otake[b], Yuko Nagakui-Noguchi[f], Miyuki Shindo[g], Mikita Suyama[c,d,e], Yasuyuki Ohkawa[c,e,h], Hideki Tsumura[g], Ken-ichirou Morohashi[b,c,1], Maki Fukami[a,1]

[a] Department of Molecular Endocrinology, National Research Institute of Child Health and Development, Tokyo 157-8535, Japan
[b] Department of Molecular Biology, Graduate School of Medical Sciences, Kyushu University, Fukuoka, Japan
[c] Department of Systems Life Sciences, Graduate School of Systems Life Sciences, Kyushu University, Fukuoka, Japan
[d] Division of Bioinformatics, Kyushu University, Fukuoka, Japan
[e] AMED-CREST, Japan Agency for Medical Research and Development, Fukuoka, Japan
[f] The National Center for Geriatrics and Gerontology, Aichi, Japan
[g] Department of Experimental Animals, National Research Institute of Child Health and Development, Tokyo, Japan
[h] Research Center for Transomics Medicine, Medical Institute of Bioregulation, Kyushu University, Fukuoka, Japan

ARTICLE INFO

Keywords:
Polycomb
Growth
Bone marrow
Adipocyte

ABSTRACT

A set of key developmental genes is essential for skeletal growth from multipotent progenitor cells at weaning. Polycomb group proteins, which regulate such genes contributes to the cell lineage commitment and subsequent differentiation via epigenetic chromatin modification and remodeling. However, it is unclear which cell lineage and gene sets are targeted by polycomb proteins during skeletal growth. We now report that mice deficient in a polycomb group gene *Cbx2*$^{cterm/cterm}$ exhibited skeletal hypoplasia in the tibia, femur, and cranium. Long bone cavities in these mice contained fewer multipotent mesenchymal stromal cells. RNA-sequencing of bone marrow cells showed downregulation and upregulation of osteoblastic and adipogenic genes, respectively. Furthermore, the expression levels of genes specifically expressed in B-cell precursors were decreased. Forced expression of Cbx2 in *Cbx2*$^{cterm/cterm}$ bone marrow stromal cell recovered fibroblastic colony formation and suppressed adipogenic differentiation. Collectively, our results suggest that *Cbx2* controls the maintenance and adipogenic differentiation of mesenchymal stromal cells in the bone marrow.

1. Introduction

Polycomb group genes were identified by genetic techniques as regulators of *Hox* genes in *Drosophila melanogaster*, and thereafter found to be phylogenetically conserved in a variety of organisms [1–3]. Subsequently, polycomb group genes were found to provide transcriptional memory through repression of *Hox* genes [4]. However, despite universally repressive activity against *Hox* genes, polycomb group proteins form discrete biochemical complexes, polycomb-repressive complex 1 (PRC1) and PRC2. Canonical PRC1 contains four core subunits: dRing, Polyhomeotic, Posterior sex comb, and Polycomb. This complex antagonizes the action of chromatin remodeling factors, thereby promoting gene silencing by chromatin compaction [5,6]. PRC2 contains Ezh2, which mediates H3K27me3 methylation [7] and likely recruits PRC1 to PRC2 target sites. Notably, mammalian PRC1 is extremely heterogeneous because each subunit has several paralogs that combinatorially assemble in a mutually exclusive fashion. For example, PRC1 in mice may form from at least six of *Posterior sex comb* homologs (*Pcgf*, *polycomb group ring finger*), three *Polyhomeotic* homologs (*Phc*, *Polyhomeotic homolog*), four *Polycomb* homologs (*Cbx*, *Chromobox*), and two RING protein homologs (*Ring finger protein 1a* and *1b*) [8].

Critically, polycomb group genes maintain cell lineage identities and cell lineage pools during differentiation [9]. For instance, PRC2 and PRC1 containing Ezh2 [10], Suz12 [11], Eed [12], Kdm2b [13], Rybp [14], and Ring1b [15] are essential for early mouse embryonic

* Corresponding author at: Department of Molecular Endocrinology, National Research Institute for Child Health and Development, 2-10-1 Okura, Setagaya, Tokyo 157-8535, Japan.
E-mail address: fukui-y@ncchd.go.jp (Y. Katoh-Fukui).
[1] Co-last authors.

https://doi.org/10.1016/j.bone.2018.10.021
Received 19 March 2018; Received in revised form 19 October 2018; Accepted 19 October 2018
Available online 30 October 2018

development at embryonic days earlier than day 10.5. In contrast, canonical PRC1 components are essential for later processes such as transformation of axial skeletal identities [16–24], hematopoietic stem cell expansion [25–29], cardiac selector gene retention [30], establishment of proper cell populations in adrenal and gonadal primordia, and sex determination [21,31,32]. In particular, *Cbx2*$^{cterm/cterm}$ (*Cbx2* nullizygous ablation by neo gene insertion) mice show defects in gonadal, adrenal, and splenic development [21,32]. XY *Cbx2*$^{cterm/cterm}$ mice develop ovaries, and the gonads are hypoplastic in both sexes [21]. Cbx2 in embryonic gonadal somatic cell regulates the expression of master transcription factor genes such as *Sry* and *Sox9* for male sex determination and *Lhx9* and *Nr5a1* for gonadal formation [31]. Intriguingly, polycomb group proteins are tethered to the loci of key regulatory genes in embryonic stem cells [33] and committed neural progenitor cells [34], perhaps suggesting that these proteins prime cell lineage commitment in later developmental stages.

During skeletal development, a sizable number of bone-building osteoblasts form from perichondrial cells and hypertrophic chondrocytes [35–37], as well as bone marrow-derived mesenchymal stromal cells, via a process regulated by the master transcription factor *Runx2* [38], while bone-absorbing osteoclasts form from hematopoietic cells. Recently, bone marrow adipocytes derived from bone marrow-derived mesenchymal stromal cells were hypothesized to function as energy reservoirs [39–41]. These cells are generated via regulation of adipogenic genes *Cebpα* and *Pparγ*, of which the latter is regarded as the master transcriptional regulator of adipocyte lineage specification [39,40,42]. The balance between osteogenesis and adipogenesis is tightly regulated, and a significant shift toward adipogenesis leads to osteoporosis [43–45]. Accordingly, the mechanisms controlling this balance are of great interest.

The role of polycomb group genes is already well-characterized in embryonic stages, but not postnatal, since knockout of such genes is lethal in mice or results in severe developmental phenotypes. Nevertheless, we previously found that *Cbx2*$^{cterm/cterm}$ mice frequently survive to adulthood despite severe growth defects [21]. To further characterize these growth defects, we investigated *Cbx2* during skeletal development at weaning.

2. Materials and methods

2.1. Cbx2 deficient mice and animal welfare

Cbx2$^{+/cterm}$, *Cbx2*$^{cterm/cterm}$, and wild type littermates were maintained in the mixed genetic background of 129 [21,31,32], which was derived from the embryonic stem cell line D3 [21] and C57BL6N (Sankyo Labo Service, Japan). Animal protocols were approved by the Animal Care Committee at the National Center for Geriatrics and Gerontology, and National Research Institute for Child Health and Development. Mice were kept specific pathogen-free in a 12-hour light-dark cycle. CA1 standard diet (Japan Clea, Japan) and water were provided ad libitum. Plasma concentration of GH and IGF-1 was measured by Luminex and ELISA respectively (FUJIFILM Wako).

2.2. Microcomputed tomography

The architecture of the proximal femur in *Cbx2*$^{cterm/cterm}$ mice and littermates was evaluated at 3 weeks by microcomputed tomography at Kureha Special Laboratory, Fukushima, Japan.

2.3. Histology

Tibias from 3-week-old *Cbx2*$^{cterm/cterm}$ mice and littermates were fixed overnight with 4% paraformaldehyde in PBS, decalcified in 15% EDTA for 10 days, embedded in paraffin, sectioned, and stained with hematoxylin and eosin. Osteoclasts were also stained using TRAP/ALP Stain Kit (294-67001, Wako Pure Chemical Industries, Osaka, Japan), and TRAP-stained cells were quantified in three sections per mouse using Image J. Sections were also stained for PCNA using rabbit polyclonal antibodies (sc-7907, Santa Cruz). Specimens were imaged on a BZ-9000 microscope (Keyence, Japan).

For immunohistochemical analyses of frozen section, newborn tibia were fixed for 15 min with 4% PFA in PBS, embedded and frozen in Tissue-Tek O.C.T Compound (Sakura Finetek Japan), sectioned and treated with 0.1% Triton X-100 in PBS, and immunostained with guinea pig antibodies to C bx2 [32] or normal guinea pig IgG (sc-2711, Santa Cruz). Antibody staining was performed in 1% skim milk and 0.1% Triton X-100 in PBS overnight at 4 °C. Biotinylated anti-guinea pig antibodies (Jackson.

Immuno Research) were used as secondary antibodies. Antigen-antibody complexes were detected using Histofine kit (Nichirei, Japan) and SIGMAFAST DAB with metal enhancer (D0426, Sigma-Aldrich). For immunocytological analyses, bone marrow stromal cells were cultured on cover glass disks (C1110, Matsunami Glass, Osaka, Japan). Cells were then fixed for 15 min with 4% PFA in PBS and treated with 0.3% Triton X-100 (93443, Sigma-Aldrich) for 30 min in PBS at room temperature. Cy3-labeled antiguinea pig antibodies (Jackson Immuno Research) were used as secondary antibodies. Antibody staining was performed in 1% skim milk and 0.3% Triton X-100 in PBS overnight at 4 °C.

2.4. Gross skeletal analyses

Head bone was prepared according to a standard protocol [46]. Briefly, skin was removed from head bones, which were then fixed for two days with 4% paraformaldehyde in PBS and cleared with 2% KOH for another two days. Subsequently, specimens were stained for two days with 50 mg/L Alizarin Red (A5533, Sigma-Aldrich) in 2% KOH, immersed in 2% KOH for 7 days, and stored in glycerol.

2.5. Colony formation assays and differentiation of bone marrow stromal cells

Tibias and femurs were collected from *Cbx2*$^{cterm/cterm}$ mice and littermates at 3 weeks, dissected, and flushed with DMEM containing 10% fetal calf serum using a 22-gauge syringe needle to harvest bone marrow cells (Terumo, Japan). To quantify colony-forming-unit fibroblasts (CFU-f), samples were dissociated into single cells and plated at 5×10^5 cells per 9.5 cm^2 in Mouse MesenCult basal medium supplemented with 20% MesenCult Supplement (Stem Cell Technologies), 100 U/mL penicillin, and 100 μg/mL streptomycin. Cells were grown at 37 °C and 5% CO_2, and media were changed every three days. After 10 days, cells were fixed overnight with 4% paraformaldehyde in PBS, and stained with nuclear staining solution (294-67001, FUJIFILM Wako, Japan or 15682, or MUTO pure chemicals, Japan). To quantify alkaline phosphatase-positive colony-forming-unit fibroblast (CFU-fap), cells were cultured in mouse MesenCult medium supplemented with 50 μg/mL ascorbic acid (A92902, Sigma-Aldrich), 10 mM β-glycerophosphate (G9891, Sigma-Aldrich), and 10^{-8} M dexamethasone (D4902, Sigma-Aldrich) (maintenance medium). Culture media were changed every 3 days, and osteoblastic cells were fixed and stained using TRAP/ALP Stain Kit (294-67001, Wako Pure Chemical Industries, Osaka, Japan) after 10 days. For Cbx2 overexpression in adipogenic and osteoblastic differentiation, passaged and pooled bone marrow stromal cells obtained from wild type (n = 3, XX = 3) or *Cbx2*$^{cterm/cterm}$ mice (n = 3, XY = 1, XX = 2) were examined. Cells were seeded into 12-well plates in maintenance medium (5×10^4 cells/well). A CAG-*Cbx2-GFP* plasmid or control *GFP* plasmid was transfected 24 h later. Media were changed every three days. For adipogenic differentiation, 3 days after transfection, adipogenesis was induced by administering maintenance medium supplemented with 0.5 mM IBMX (3-isobutyl-1 methylxanthine) (I5879, Sigma-Aldrich), 5 μg/mL insulin (I6634, Sigma-Aldrich), 1 μM rosiglitazone (ab120762, Abcam) and 0.25 μM

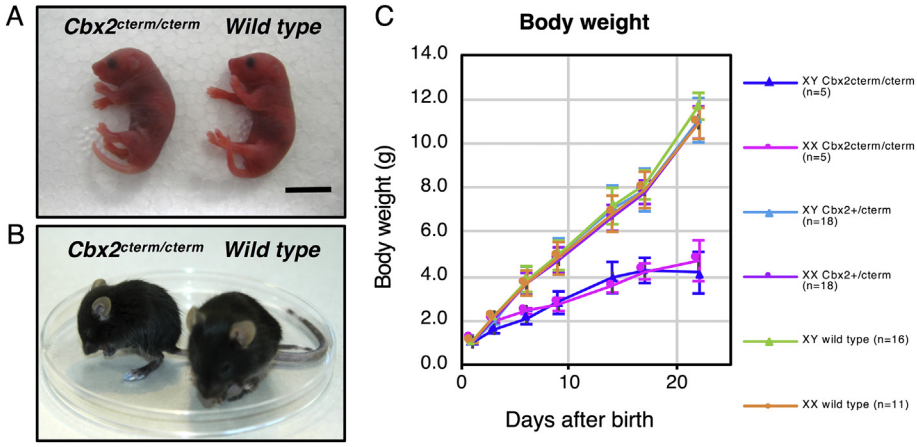

Fig. 1. Growth defects in postnatal *Cbx2*$^{cterm/cterm}$ mice. (A) Surviving newborn *Cbx2*$^{cterm/cterm}$ mice (left), with comparable size as wild type littermates (right). Scale bar, 5 mm. (B) *Cbx2*$^{cterm/cterm}$ (left) were smaller than wild type littermates (right) at 3 weeks. (C) *Cbx2*$^{cterm/cterm}$ mice were significantly lighter than *Cbx2*$^{+/cterm}$ and wild type littermates at 7 days, and especially at 3 weeks.

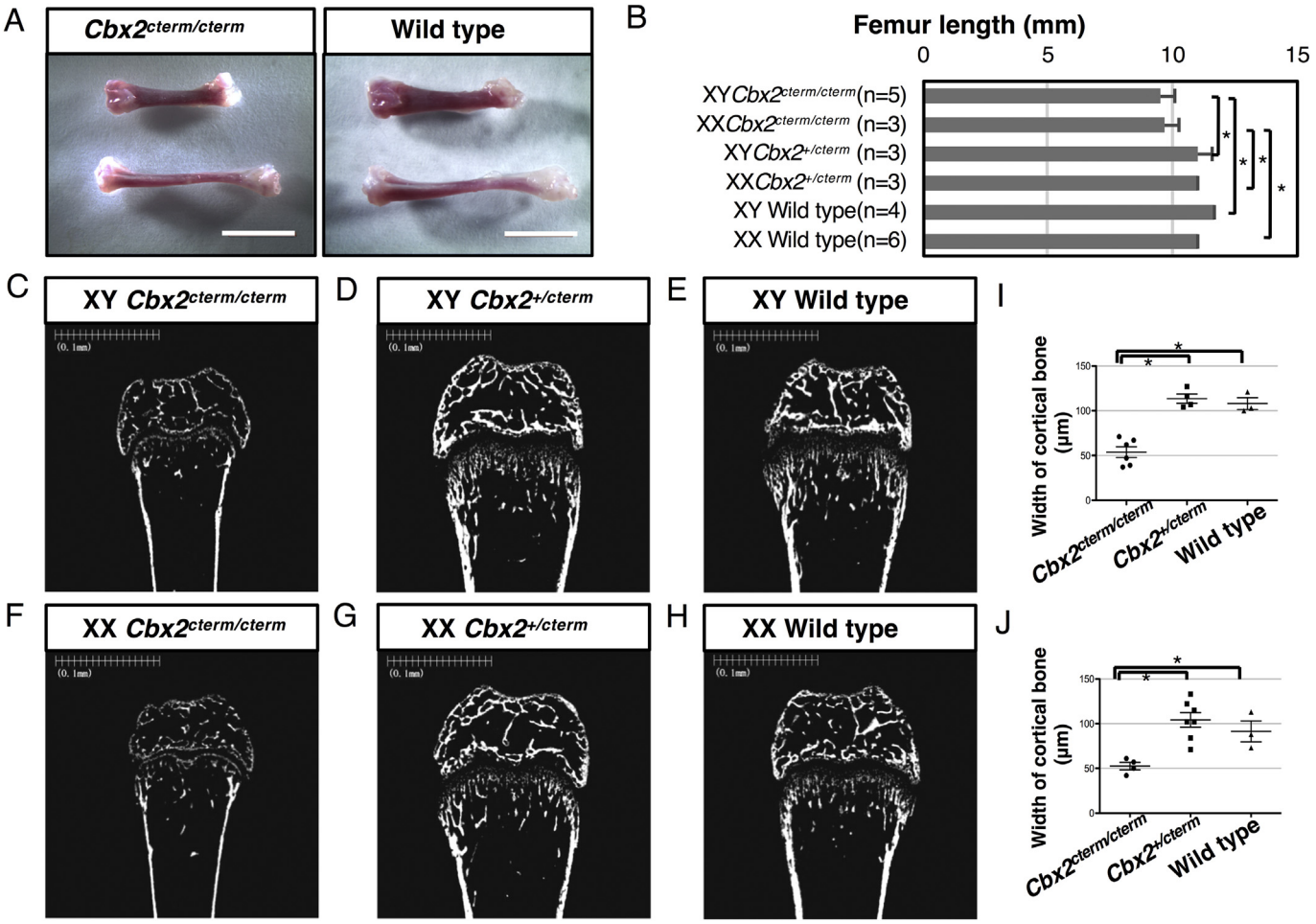

Fig. 2. Structural abnormalities in *Cbx2* nullizygous long bones. (A) Femurs and tibias were shorter at 3 weeks in *XY Cbx2*$^{cterm/cterm}$ mice than in wild type littermates. Scale bars, 0.5 mm. (B) Femoral length in *Cbx2*$^{cterm/cterm}$, *Cbx2*$^{+/cterm}$, and wild type littermates of both sexes. (C–H) Microcomputed tomography, at Kureha Special Laboratory, Fukushima, Japan, of the proximal femur in XY *Cbx2*$^{cterm/cterm}$ (C), XY *Cbx2*$^{+/cterm}$ (D), XY wild type (E), XX *Cbx2*$^{cterm/cterm}$ (F), XX *Cbx2*$^{+/cterm}$ (G), and XX wild type littermates (H). The scans reveal thinner cortical (I–J) and sparse trabecular bone in *Cbx2*$^{cterm/cter}$ mice. Data are mean ± SD. *, $p < 0.05$. (K–R) Femoral bone density per bone volume in XY (K) and XX (L) mice of indicated genotypes, showing significant reduction in *Cbx2*$^{cterm/cterm}$ mice of both sexes. Although trabecular thickness in femoral bone of XY and XX *Cbx2*$^{cterm/cterm}$ mice was similar to wild type female type (M–N), trabecular numbers (O–P) and trabecular spaces (Q-R) in femoral bone were significantly reduced in *Cbx2*$^{cterm/cter}$ mice of both sexes. Center lines represent medians, upper and lower lines represent the 25th and 75th percentile, respectively, and whiskers indicate range. *, $p < 0.05$; **, $p < 0.01$.

dexamethasone (D4902, Sigma-Aldrich) for 14 days. For osteoblastic differentiation, 2 days after transfection, osteogenesis was induced by administering maintenance medium supplemented with 50 μg/mL ascorbic acid (A92902, Sigma-Aldrich), 10 mM β-glycerophosphate (G9891, Sigma-Aldrich), and 10 nM dexamethasone (D4902, Sigma-Aldrich) for 6 days.

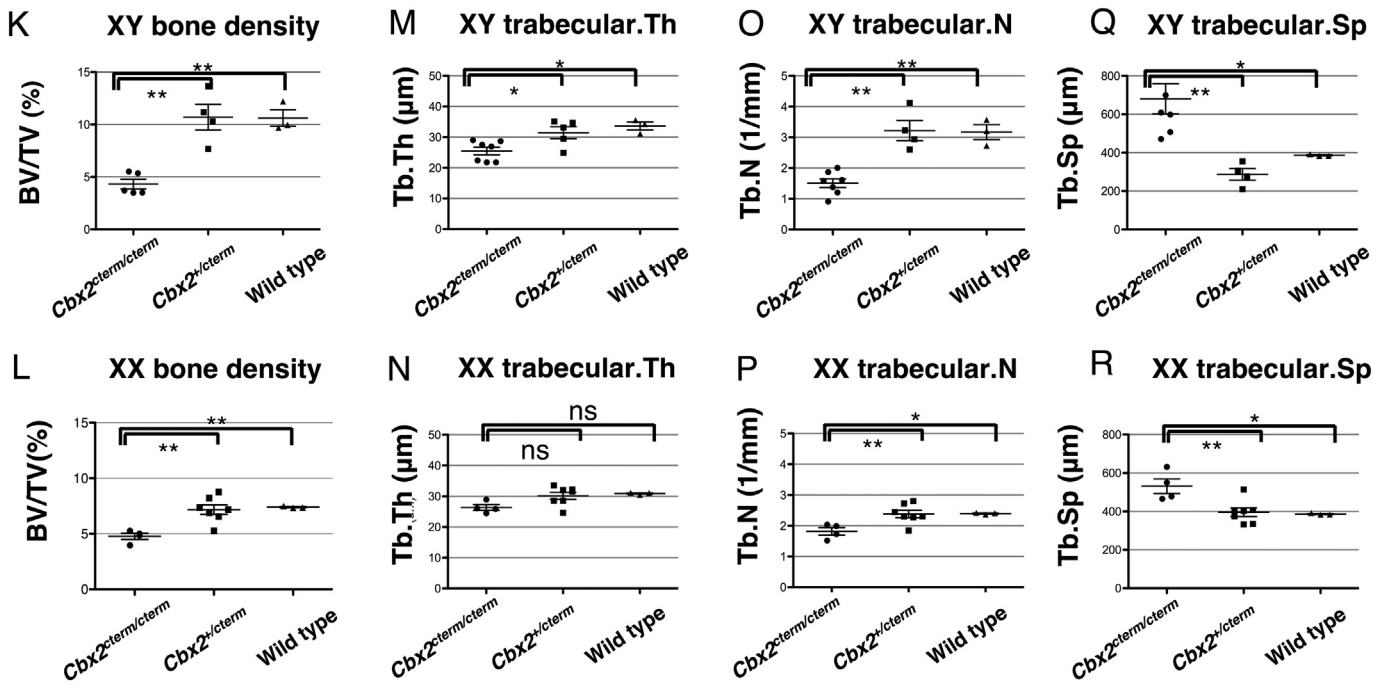

Fig. 2. (*continued*)

2.6. Real-time reverse transcriptase PCR (RT-qPCR) assay

RNA was isolated from cells using the RNeasy Mini Kit (74104, Qiagen) and RNase-Free DNase Set (79254, Qiagen). The isolated 200 ng of total RNA was reverse transcribed into cDNA with random primer using the High-Capacity RNA-to-cDNA™ Kit (4387406, Thermo Fisher Scientific). cDNA was quantified using the real-time PCR machine Fast 7000 (Thermo Fisher Scientific) and Fast SYBR® Green Master Mix (4385612, Thermo Fisher Scientific). RNA levels were quantified using the relative quantification method and normalized to the housekeeping gene *Gapdh*. Primers used in this study were as follows; ***Gapdh*** (fw: AAC TTT GGC ATT GTG GAA GG, rv: ACA CAT TGG GGG TAG GAA CA), ***Cbx2*** (fw: GGC TGG TCC TCC AAA CAC AA, rv: CCC TGG GTC TCT TGC CTC T), ***Pparγ2*** (fw: CGC TGA TGC ACT GCC TAT GA, rv: AAT GGC ATC TCT GTG TCA ACC A), ***Ocn*** (fw: CTT GGT GCA CAC CTA GCA GA, rv: ACC TTA TTG CCC TCC TGC TT).

2.7. mRNA sequencing

Total RNA was prepared using RNeasy Mini Kit (74104, Qiagen) and RNase-Free DNase Set (79254, Qiagen) from tibial and femoral bone marrow obtained from 3-week-old $Cbx2^{cterm/cterm}$ (n = 3, average body weight 4.0 g) and wild type mice (n = 3, average body weight 12.3 g). Libraries were constructed using TruSeq Stranded mRNA Sample Prep Kit (Illumina, San Diego, CA, USA) according to the manufacturer's standard protocol, and sequenced by 50 bp single-end sequencing on Illumina HiSeq 1000. Reads were checked for quality in FASTQC version 0.11.5 [47] and mapped to the reference mouse genome UCSC version mm10 using the option '-library-type fr-secondstrand' in TopHat version 2.1.0 [48]. Transcripts were then assembled in Cufflinks version 2.2.1 [49] using option '-u-library-type fr-secondstrand', and expression was calculated as fragments per kilobase of exon per million mapped fragments (FPKM). To identify differentially expressed genes, a threshold of 0.001 was set for the *q*-value calculated by Cuffdiff in the Cufflinks package, leaving 1430 genes in the final data set. mRNA-seq data were deposited in Gene Expression Omnibus under the accession number GSE112227.

Genes expressed with FPKM > 10 in wild type mice but also > 4-fold more abundant in $Cbx2^{cterm/cterm}$ mice (42 genes) were selected for further analysis, along with 76 genes with FPKM > 10 in the former but expressed < 0.25-fold on average in the latter. All these genes were annotated in Database for Annotation Visualization and Integrated Discovery 6.8 (http://david.abcc.ncifcrf.gov/) [50,51] respectively. Enriched biological processes and KEGG pathways were selected based on *p*-value < 0.01.

2.8. Statistics

Groups were compared by unpaired Student's *t*-test or ANOVA followed by Newman-Keuls Multiple Comparison Test (GraphPad Prism, USA). *p*-Values < 0.05 were considered significant, and are marked * for $p < 0.05$, ** for $p < 0.01$, and ns for not significant.

3. Results

3.1. Postnatal growth failure in Cbx2 nullizygous mice

In a mixed 129/C57BL/6 genetic background, $Cbx2^{cterm/cterm}$ mice are born alive at a rate of 5% by intercrossing heterozygous $Cbx2^{+/cterm}$ mice. This ratio suggests that approximately 80% of $Cbx2^{cterm/cterm}$ mice die perinatally. The mortality increased to 100% in a C57BL/6 genetic background. Although newborn $Cbx2^{cterm/cterm}$ were similar in size to wild type littermates (Fig. 1A), they looked smaller 7 days after birth. Their weights were < 50% of wild type at 3 weeks (Fig. 1B, C). The decreased body weight was observed in both sexes. There was no obvious difference in body weight between heterozygous $Cbx2^{+/cterm}$ and wild type littermates at any age.

3.2. Structural abnormality in Cbx2 nullizygous femurs

Consistent with the decrease in body weight, the femurs and tibias appeared to be shorter in $Cbx2^{cterm/cterm}$ mice at 3 weeks after birth (Fig. 2A). Indeed, the femurs of $Cbx2^{cterm/cterm}$ mice of both sexes were significantly shorter than those of wild type and heterozygous mice (Fig. 2B) and were often modestly twisted. However, clinodactyly, shortness in front legs, and shortness in clavicles were not observed (data not shown). Microcomputed tomography of distal femurs in 3-week-old mice also revealed significantly thinner cortical bone

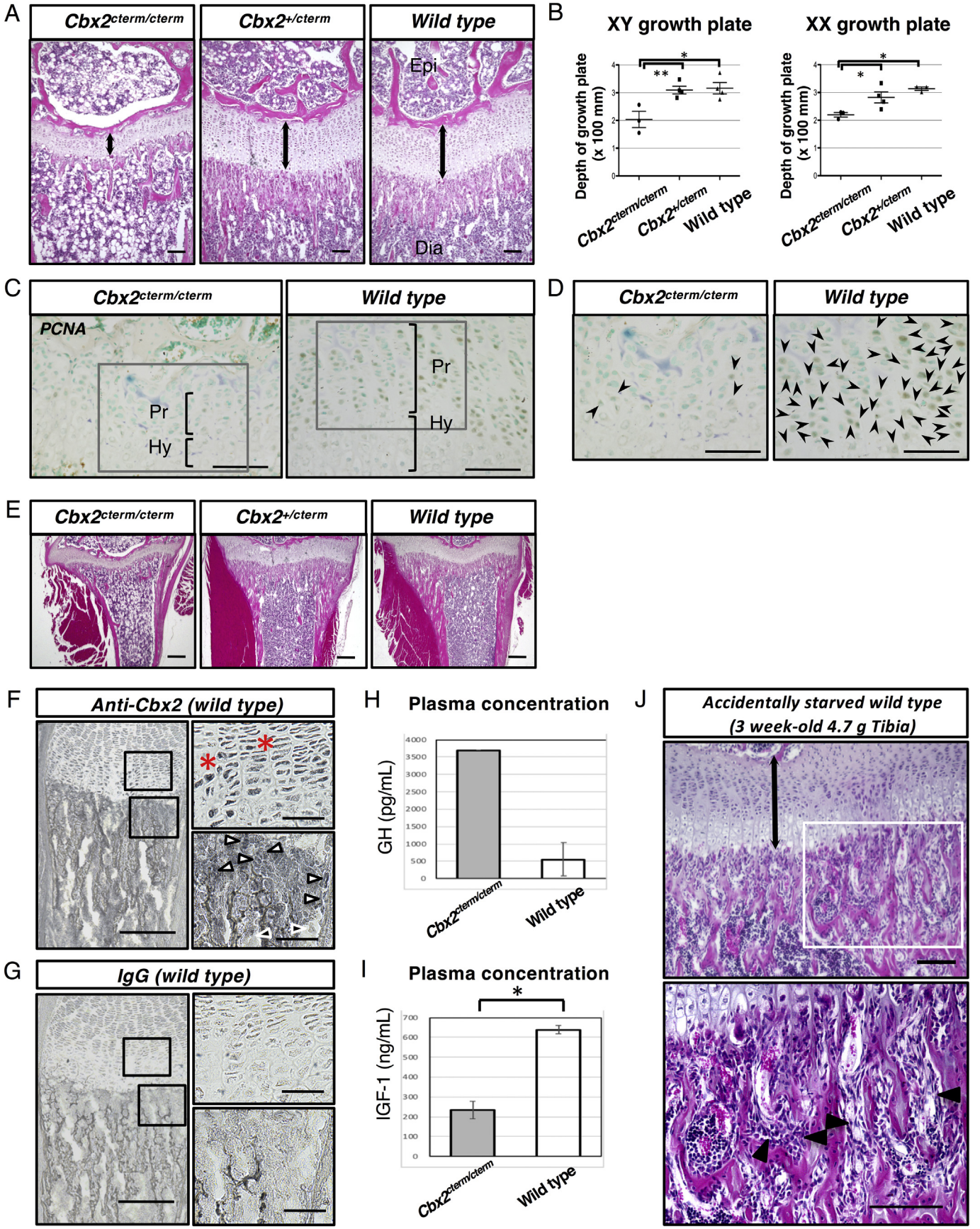

(caption on next page)

Fig. 3. Histology of proximal tibiae at 3 weeks. (A) Hematoxylin and eosin staining shows poor trabecular structure in XY *Cbx2*$^{cterm/cterm}$ mice, in comparison to XY *Cbx2*$^{+/cterm}$ and XY wild type littermates. Furthermore, adipocytes prominently expanded in the bone marrow cavity of *Cbx2*$^{cterm/cterm}$ mice. Arrows indicate depth of the growth plate. Epi, epiphysis; Dia, diaphysis. Scale bars, 100 μm. (B) Reduced growth plate depth in *Cbx2*$^{cterm/cterm}$ mice (n = 3 XY and n = 3 XX) in comparison to *Cbx2*$^{+/cterm}$ (n = 4 XY and n = 4 XX) and wild type littermates (n = 4 XY and n = 3 XX). Center lines are medians, upper and lower lines are the 25th to 75th percentile, respectively, and whiskers indicate range. *, $p < 0.05$; **, $p < 0.01$. (C, D) Rare PCNA-stained nuclei (arrowheads in D) in XY *Cbx2*$^{cterm/cterm}$ mice, in comparison to XY wild type littermates. Square brackets indicate the width of growth plates. Pr, proliferating zone; Hy, hypertrophic zone. Scale bars, 100 μm (C) and 50 μm (D). (E) Low-power field hematoxylin and eosin staining of sections from XY *Cbx2*$^{cterm/cterm}$, XY *Cbx2*$^{+/cterm}$, and XY wild type littermates. Scale bars, 250 μm. (F, G) Immunostaining of specimens from new born tibia using Cbx2 antibody. Asterisks indicate cells in chondrocyte lineage in the proliferating zone. White arrows heads indicate osteoblastic lineage cells. Black arrows heads indicate osteoclastic cells. Scale bars, 100 μm (left panels in F and G) and 25 μm (right panels in F and G). (H) Plasma concentration of GH (pg/mL). Data are mean ± SD. Because of the small blood sample from *Cbx2*$^{cterm/cterm}$, serum was pooled from 3 mice (XY = 1, XX = 2). (I) Plasma concentration of IGF-1 (ng/mL). Data are mean ± SD. *, $p < 0.05$. (J) Hematoxylin and eosin staining of sections of tibia from accidentally starved wild type mice. The lower panel shows high power field. Arrow indicates depth of the growth plate. Arrowheads indicate the osteoblastic lineage cells. Scale bars, 100 μm.

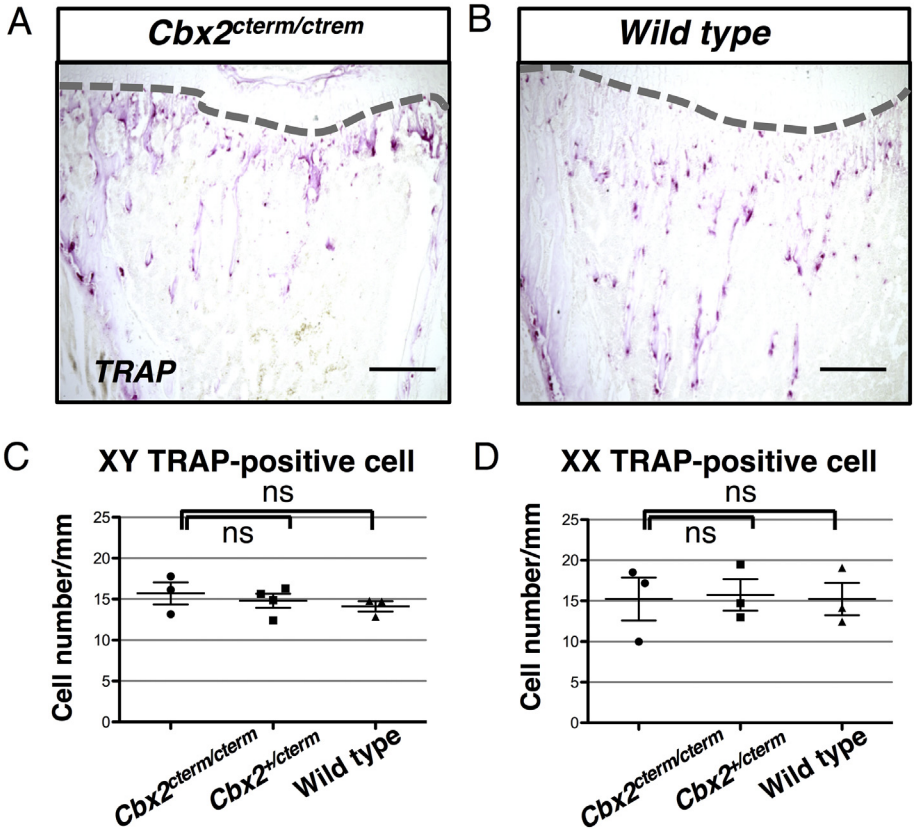

Fig. 4. Histology of osteoclast cells in the proximal tibia of *Cbx2*$^{cterm/cterm}$ mice at 3 weeks. (A, B) TRAP staining of sections from XY *Cbx2*$^{cterm/cterm}$ (A) and XY wild type littermates (B). Dashed lines mark the edges of growth plates. Scale bars, 100 μm. (C, D) Comparable TRAP-positive cells per bone perimeter in the proximal tibial cavity of *Cbx2*$^{cterm/cterm}$ (n = 3 XY and n = 4 XX), *Cbx2*$^{+/cterm}$ (n = 4 XY and n = 4 XX), and wild type littermates (n = 3 XY and n = 4 XX). Center lines are medians, upper and lower lines are the 25th and 75th percentile, respectively, and whiskers indicate range. ns, not significant.

(Fig. 2C–J), less dense trabecular bone (Fig. 2K, L), female type trabecular thickness (Fig. 2M, N), less trabecular number (Fig. 2O, P) and more trabecular space (Fig. 2Q, R) in *Cbx2*$^{cterm/cterm}$ animals of both sexes.

3.3. Hypoplasia in growth plate, long bone cavity, and cortical bone in Cbx2 nullizygous tibias

As shown in Fig. 3A, a growth plate is formed between the primary (diaphysis) and secondary ossification centers (epiphysis) in the proximal tibia of 3-week-old wild type mice. This plate consists of multiple layers of cells that promote longitudinal growth of the long bone in weaning-age mice through cell proliferation, secretion of extracellular matrix, and hypertrophy of chondrocytes. The growth plate was thinner and disorganized in *Cbx2*$^{cterm/cterm}$ mice (Fig. 3A, B). Accordingly, fewer proliferating PCNA-positive nuclei were observed in these bones (Fig. 3C, D). As TUNEL-positive apoptotic cells were rarely detected in proliferating and hypertrophic zones (data not shown), the defects in the growth plate may reflect loss of proliferation in the proliferating zones. Moreover, *Cbx2*$^{cterm/cterm}$ mice formed poor trabecular structures (Fig. 3A, E) in the tibia, as was observed by microcomputed tomography of femurs. In contrast, adipocyte expansion was clearly observed in the bone marrow cavity of tibias (Fig. 3A, E). Nuclear Cbx2 expression was detected in the cells in the proliferating zone of the growth plate (asterisk) and osteoblasts at the bone periphery (white arrow heads), but not detected in osteoclasts in wild type new born proximal tibia (black arrow heads) (Fig. 3F). No signals were observed with staining by normal IgG (Fig. 3G). Taken together, *Cbx2* ablation of the growth plate defect leads to a shorter and modestly twisted long bone and presumably short stature of *Cbx2*$^{cterm/cterm}$ mice. To examine endocrine disorder growth deficiency, plasma concentration of GH and IGF-1 was measured in 3-week-old *Cbx2*$^{cterm/cterm}$ mice. Nearly 6-folds GH elevation and 70% IGF-1 reduction were observed (Fig. 3H, I). Diet intake difficulties of *Cbx2*$^{cterm/cterm}$ mice would contribute to this IGF-1 reduction. Consistently, the glucose concentration in serum at 1 week was normal, but was almost 60% of those of wild type littermates at 3 weeks (n = 3). However, thinner growth plate and osteoporotic phenotypes, such as increased adipocyte in bone marrow were not detected by histological analyses in accidentally starved wild type mice (with almost 60% decrease in body weight) (Fig. 3J).

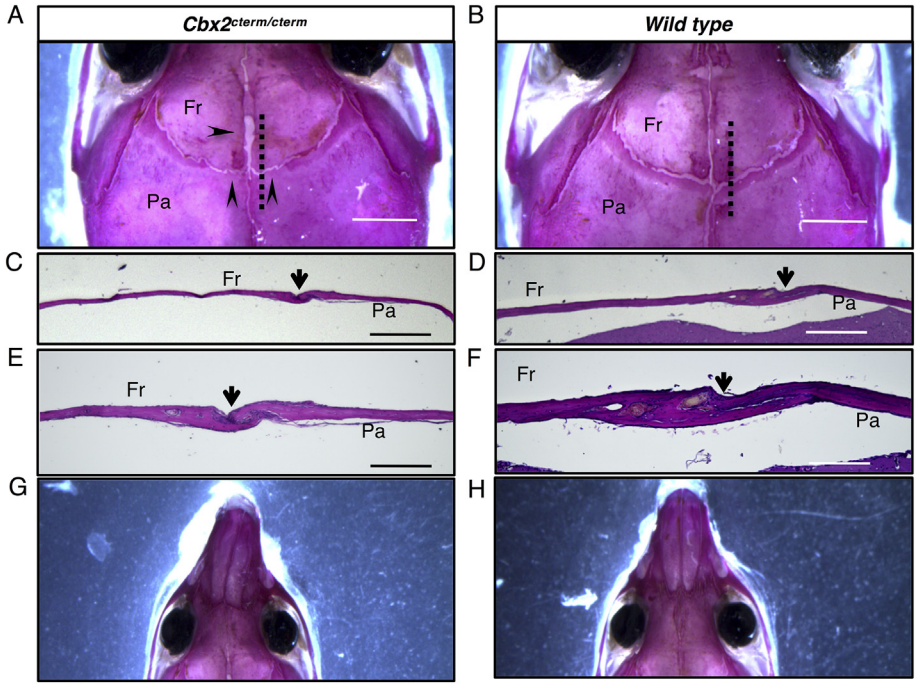

Fig. 5. Analyses of the head bone in *Cbx2*$^{cterm/cterm}$ mice at 3 weeks. (A, B) Overall appearance of transparent skeletal specimens showing the frontal bone (Fr) and parietal bone (Pr) in *Cbx2*$^{cterm/cterm}$ (A) and wild type littermates (B). Alizarin red staining revealed underdevelopment at parietal regions of the coronal and frontal suture (arrowheads). Dashed lines indicate approximate positions of parasagittal sections shown in C–F. Scale bars, 2 mm. (C–F) Parasagittal sections show thinner frontal and parietal bones in *Cbx2*$^{cterm/cterm}$ mice (C, E), in comparison to wild type littermates (D, F). Arrows indicate coronal sutures. Scale bars, 200 μm (C, E) and 100 μm (D, F).

Since both bone-forming osteoblasts and bone-absorbing osteoclasts are required for trabecular formation, we tested for TRAP-positive osteoclasts in the bone cavity and found that the number of these cells was comparable at 3 weeks between *Cbx2*$^{cterm/cterm}$ and wild type mice of both sexes (Fig. 4A–D).

3.4. Hypoplasia in cranial bones

While endochondral ossification occurs in long bone trabeculae, the cranial bone undergoes intramembranous ossification, in which condensed mesenchymal cells are directly ossified. Alizarin Red staining of the cranial bone showed underdeveloped sutures at the coronal and frontal parietal regions in 3-week-old *Cbx2*$^{cterm/cterm}$ mice (n = 4/4, arrowheads in Fig. 5A), although craniosynostosis and doming were not observed. In particular, parasagittal sections of coronal sutures (broken lines in Fig. 5A, B) showed that the frontal and parietal bones were thinner and that the coronal suture was hypoplastic in comparison to those in wild type littermates (n = 3/3, Fig. 5C–F). These defects were not observed in *Cbx2*$^{+/cterm}$ littermates (n = 3/3), suggesting that *Cbx2* on both alleles are essential for both proper intramembranous and endochondral ossification. In addition, malocclusions associated with twisting nasal bones were observed in *Cbx2*$^{cterm/cterm}$ mice (n = 5/15) (Fig. 5G, H).

3.5. Cbx2 nullizygous ablation diminishes bone marrow stromal cell density and osteoblastic differentiation capacity

Colony-forming unit fibroblasts, which are a measure of self-renewal in mesenchymal stem or progenitor cells in the bone marrow, were significantly diminished in *Cbx2*$^{cterm/cterm}$ mice of both sexes (Fig. 6A, B, E), as were colony-forming osteoblasts that express alkaline phosphatase, which are a measure of osteogenic capacity (Fig. 6C–E). These results suggest that *Cbx2* maintains the abundance of stem and progenitor cells in the bone marrow. Actually, immunocyte chemistry of bone marrow stromal cells showed nuclear localization of Cbx2 (Fig. 6F).

3.6. Effect of Cbx2 nullizygous ablation on gene expression in the postnatal long bone cavity

Since Cbx2 is a component of PRC1, we anticipated that *Cbx2* ablation would affect expression of master developmental genes of cells in bone tissue. Hence, we obtained the transcriptome of tibial and femoral bone marrow cells harvested from 3-week-old *Cbx2*$^{cterm/cterm}$ (n = 3) and wild type littermates (n = 3). Differentially expressed genes were then subjected to Gene ontology or KEGG pathway analyses to reveal which cellular functions were affected. Notably, *Cbx2* ablation upregulated genes associated with the gene ontology terms ‘gluconeogenesis’, ‘aging’, ‘NADH oxidation’, and ‘response to peptide hormone’, which are consistent with adipocyte function. On the other hand, genes associated with ‘collagen fibril organogenesis’ and ‘ossification’, which are closely related to bone differentiation, were downregulated (Fig. 7A, C and Table S1). Similarly, KEGG pathways related to adipogenesis, including ‘glucolysis/gluconeogenesis’ and ‘PPAR signaling pathway’, were upregulated, while those related to bone differentiation, including ‘protein digestion and absorption’ and ‘ECM-receptor interaction’, were repressed. In addition, ‘B cell receptor signaling pathway’ and ‘primary immunodeficiency’, which are linked to differentiation of B-cell progenitors, were downregulated (Fig. 7B, D and Table S2).

Consistent with adipocyte accumulation in *Cbx2*$^{cterm/cterm}$ bones, the expression of the adipocyte-specific gene *Fabp4* and its regulators *Cebpα* and *Pparγ2* was elevated. In contrast, the expression of osteoblastic-specific genes *Sp7/Osx*, *Alpl*, *Bglap/Ocn*, and collagen genes, was decreased. Interestingly, however, the expression of *Runx2*, the most upstream master regulator of osteoblast, did not show marked differences between *Cbx2*$^{cterm/cterm}$ mice and wild type mice (Fig. 7E). These observations suggest that decreased and increased expression of genes associated with osteoblasts and adipocytes, respectively, may account for the osteoporotic phenotype of *Cbx2*$^{cterm/cterm}$ mice.

3.7. Rescue experiment by forced expression of Cbx2 in bone marrow stromal cell derived from *Cbx2*$^{cterm/cterm}$ mice

Cbx2 overexpression using *CAG* promoter was performed in bone marrow stromal cells to examine the cause-and-effect relationship between the loss of Cbx2 and phenotypes. Colony numbers of fibroblasts

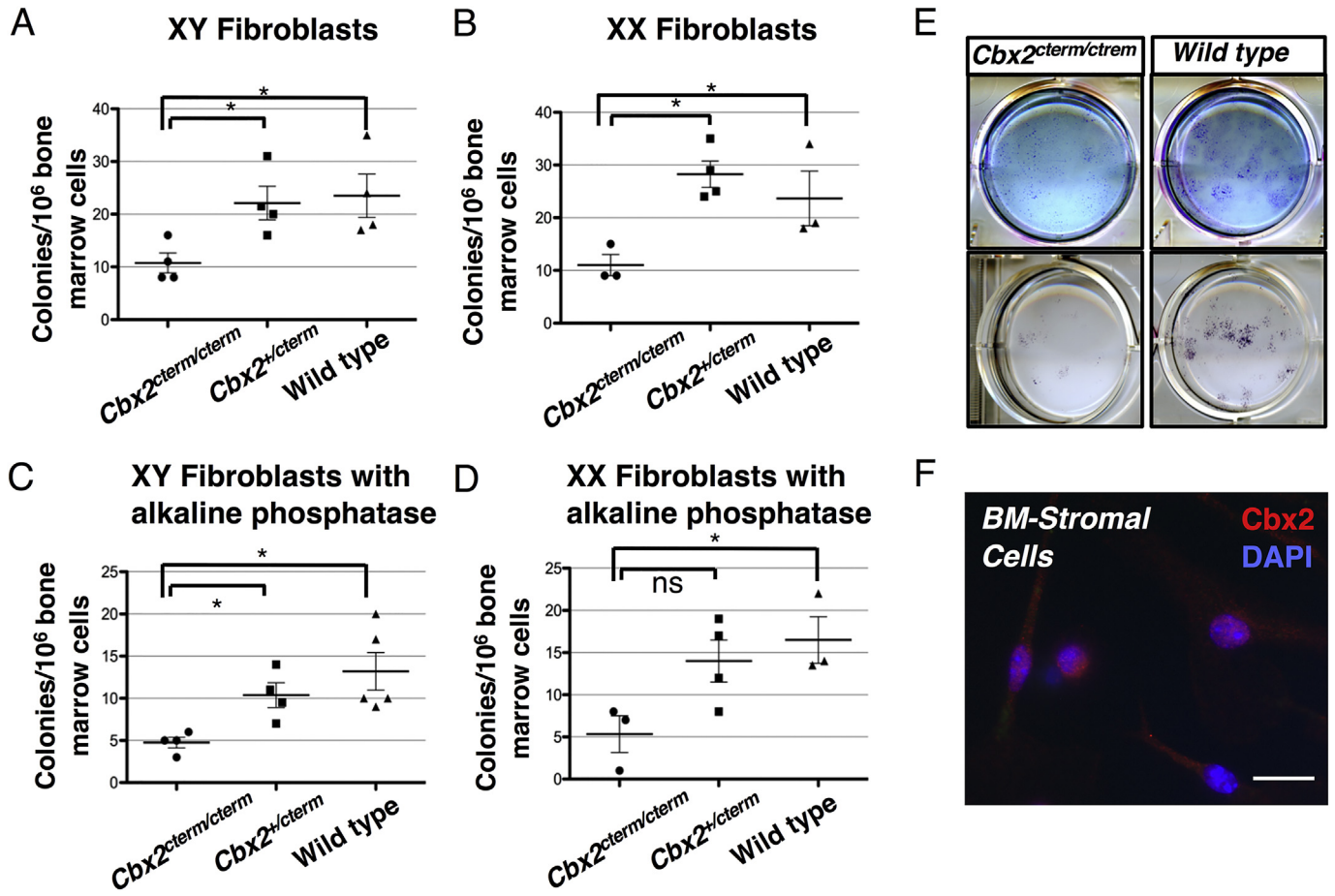

Fig. 6. Colony-forming fibroblasts and colony-forming fibroblasts expressing alkaline phosphatase in 3-week-old mice. (A, B) Colony-forming fibroblasts were significantly fewer per 10^6 bone marrow cells in femurs and tibias from *Cbx2*$^{cterm/cterm}$ mice (n = 4 XY and n = 4 XX), in comparison to *Cbx2*$^{+/cterm}$ (n = 4 XY and n = 4 XX) and wild type littermates (n = 4 XY and n = 5 XX). Center lines are medians, upper and lower lines are the 25th and 75th percentile, respectively, and whiskers indicate the range. Data are mean ± SD. *, $p < 0.05$; ns, not significant. (C, D) Colony-forming fibroblasts expressing alkaline phosphatase were also significantly fewer per 10^6 bone marrow cells in femurs and tibias of *Cbx2*$^{cterm/cterm}$ mice (n = 4 XY and n = 4 XX), in comparison to *Cbx2*$^{+/cterm}$ (n = 4 XY and n = 4 XX) and wild type littermates (n = 5 XY and n = 5 XX). Center lines are medians, upper and lower lines represent are the 25th and 75th percentile, respectively, and whiskers indicate the range. Data are mean ± SD. *, $p < 0.05$; ns, not significant. (E, F) Representative colony-forming fibroblasts (E upper low) and colony-forming fibroblasts with alkaline phosphatase (E lower low) from XY *Cbx2*$^{cterm/cterm}$ and XY wild type littermates. (F) Immunocytochemistry of wild type bone marrow stromal cells using Cbx2 antibody. Scale bars, 20 μm.

were recovered by forced expression of *Cbx2* (Fig. 8A). Moreover, passaged and pooled bone marrow stromal cells were forced to express *Cbx2* and cultured in a medium for adipogenic differentiation (Fig. 8B, C). *Cbx2* expression levels were > 50-fold of wild type at 48 h after transfection (Fig. 8B). Consistent with the in vivo data, in the medium for adipogenic differentiation, the expression levels of *Pparγ2* were > 2-folds higher in bone marrow stromal cells derived from *Cbx2*$^{cterm/cterm}$ mice than in those derived from wild type mice. Moreover, surprisingly, the expression levels of *Pparγ2* were reduced to less than half in bone marrow stromal cells by Cbx2 forced expression (Fig. 8C). In the medium for osteoblastic differentiation, forced expressed levels of *Cbx2* were almost 100-fold of wild type at 48 h after transfection (Fig. 8D). However the expression levels of *Ocn* in cells derived from *Cbx2*$^{cterm/cterm}$ mice could not restored by the forced expression of Cbx2 (Fig. 8E).

4. Discussion

4.1. Comparison of skeletal phenotypes among polycomb group gene deficient mice

Knockout of various polycomb group genes elicits striking phenotypes in long bones. Indeed, knockout mice for the canonical PRC1 subunit Pcgf4/Bmi1 [52], the PRC2 subunit Ezh2 [53], and the *Polycomb* enhancer *Asxl1*, which genetically interacts with *Cbx2* [44], displayed osteogenetic defects in postnatal long bones. We now demonstrate for the first time the involvement of *Cbx2* in postnatal bone formation. Similar to *Pcgf4/Bmi1* nullizygous mice [52], *Cbx2*$^{cterm/cterm}$ mice showed osteopenic and fatty bone marrow phenotypes, although the affected cell lineage remains to be elucidated. *Ezh*$^{fl/fl}$;*Prrx1-cre* mice, in which *Ezh2* is depleted from mesenchymal progenitor cells (*Ezh2*$^{fl/fl}$;*Prrx1-cre* mice) [53], and *Asxl*$^{fl/fl}$;*Osx-cre* mice, in which *Asxl1* is depleted from multipotent mesenchymal progenitor cells [44] showed a severe osteopenic bone and fatty bone marrow. These reports indicate that at least some polycomb group genes are essential for differentiation of mesenchymal progenitor cells in postnatal long bone, although the effector loci remain unknown.

Polycomb group genes appear to have different roles in postnatal craniofacial bone formation. In *Asxl*$^{fl/fl}$;*Osx-cre* mice, hypoplastic supraorbital ridges are observed, while craniosynostosis occurs in *Ezh2*$^{fl/fl}$;*Prrx1-cre* mice. In mice in which *Ezh2* is ablated from neural crest cells (*Ezh2*$^{fl/fl}$;*Wnt1-cre* mice) [54], bone and cartilage are entirely absent from the craniofacial region. In contrast, *Cbx2*$^{cterm/cterm}$ mice formed underdeveloped sutures instead, implying defects in the mesenchymal cells involved. In addition, malocclusions were observed in *Cbx2*$^{cterm/cterm}$ mice, which have not been reported for any other knockout mouse of polycomb group genes, suggesting that individual polycomb group

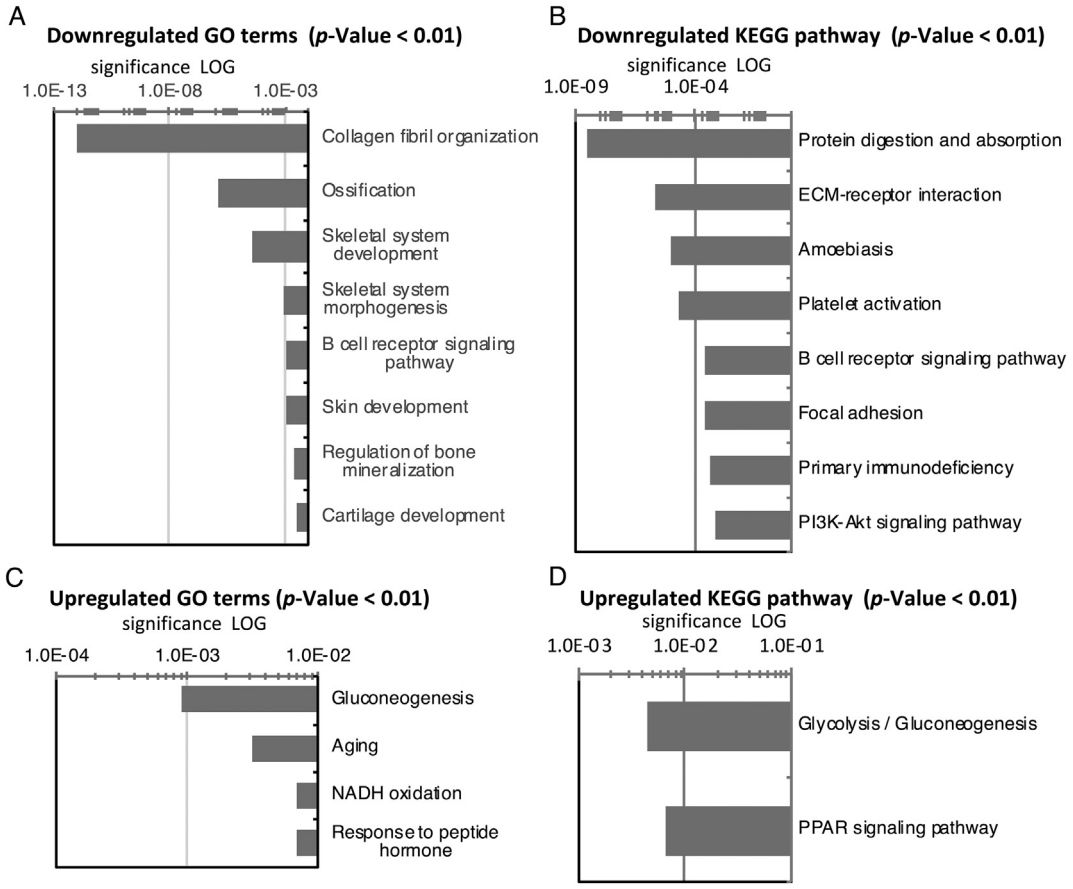

Fig. 7. Differentially expressed genes in *Cbx2*$^{cterm/cterm}$ mice, as assessed by RNA sequencing and gene ontology and KEGG pathways analysis in DAVID 6.8 (https://david.ncifcrf.gov/). (A) Top downregulated gene ontology terms are associated with osteogenesis. (B) Top downregulated KEGG pathways include 'protein digestion and absorption,' which is related to bone differentiation. (C) Top upregulated gene ontology terms include terms related to adipogenesis. (D) Top upregulated KEGG pathways include 'PPAR signaling pathway', which is related to adipogenesis. (E) Expression of adipogenic, osteoblastic, and B-cell lineage genes, in fragments per kb of exon per million mapped reads (FPKM). The adipogenic gene *Fabp4* and its regulators were upregulated *Cbx2*$^{cterm/cterm}$ mice, while osteoblast-specific genes were downregulated, although the master osteogenic regulator Runx2 was not altered. Data are mean ± SD. *, $p < 0.05$; **, $p < 0.01$; ns, not significant.

genes have different functions in specific craniofacial bones. Indeed, tissue-specific phenotypes in knockout mice of polycomb group genes are of great interest because of the heterogeneity in the origin of the head bone.

4.2. Endocrine factors affect small-sized Cbx2 deficient mice

Cbx2$^{cterm/cterm}$ mice seems to have food intake difficulties presumably because of small body size compare with the other litter siblings. Indeed IGF-1 levels in serum were significantly decreased in *Cbx2*$^{cterm/cterm}$ mice. Acid labile subunit (IGF-1 carrier protein) knockout mice showed ~65% reduction in serum IGF-1, which was associated with 30–40% decrease in body weight [55]. Therefore, low level of IGF-1 may cause weight loss observed in *Cbx2*$^{cterm/cterm}$ mice; however, the effect will be restricted. However, a thinner growth plate and osteoporotic phenotype, such as the increased adipocytes in the bone marrow were not detected in accidentally starved wild type mice (with ~60% decrease in body weigh) (Fig. 3J). Because Cbx2 was expressed in growth plates and osteoblastic lineages in new born mice (Fig. 3F), it is possible that Cbx2 autonomously contributes to bone growth in the postnatal period.

4.3. mRNA sequencing revealed bone marrow cell lineages impacted by nullizygous Cbx2 deletion

mRNA sequencing of the bone marrow in long bones revealed that genes essential for differentiation for osteoblasts, early B-cells, and adipogenic cells were dysregulated in 3-week-old *Cbx2*$^{cterm/cterm}$ mice. In particular, the data suggest that *Cbx2* represses adipogenic genes and promotes the expression of genes associated with osteoblastic and lymphoid cells. PRC1 is generally thought to repress gene expression. However, recently, PRC1 mediated activation indicates a novel function of PRC1 in development, as has been reported in a group of sperm lineage genes or limb forming genes [56,57]. Therefore, it is possible that Cbx2 positively regulates osteoblast and B-cell lineage.

The other possible factor provoking the dysregulation of a set of genes in *Cbx2*$^{cterm/cterm}$ mice is the mutual regulation between lineages. Indeed, accumulating evidence suggests that commitment of bone marrow mesenchymal stromal cells to adipogenic or osteoblastic lineages is reciprocally balanced in vivo [44,52,53].

Whether the defects in the differentiation of lymphoid cells influence adipogenic and osteoblastic differentiation, or vice versa, remain to be established. In contrast, lymphocyte-specific overexpression of *Pcgf4/Bmi1* stimulates skeletal formation [58], thus linking hematopoietic regulation to skeletal formation. Accordingly, future studies should examine whether the reduction in lymphoid cells in *Cbx2*-deficient bone marrow is an intrinsic or an indirect effect, perhaps by ablation of *Cbx2* in specific lineages. Of note, CXCL12-abundant reticular cells, which are also a constituent of bone marrow mesenchymal stromal cells, were recently found to accelerate the maturation of lymphoid progenitor cells through cell-cell interactions and cytokine production [59].

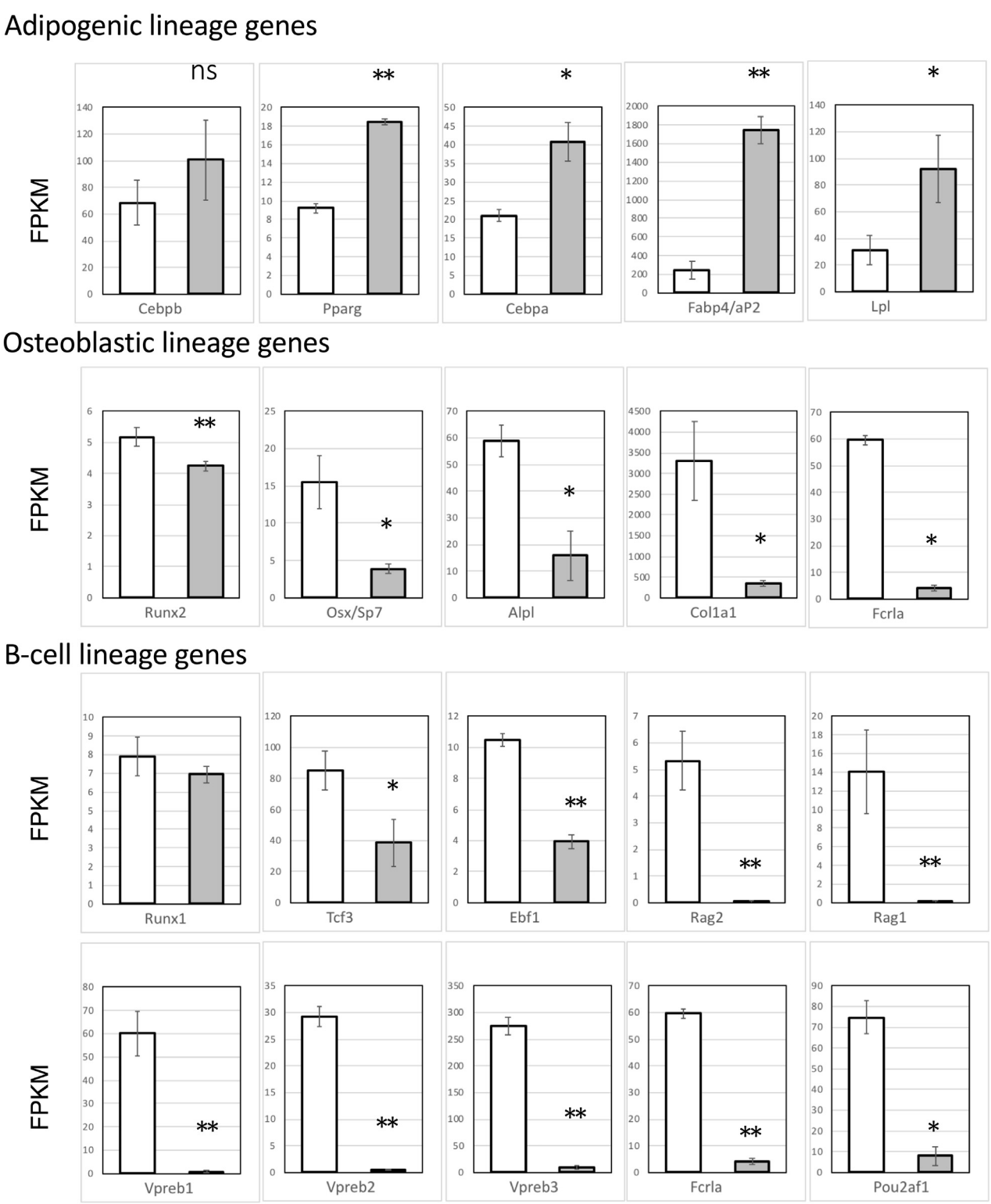

Fig. 7. (*continued*)

4.4. Role of polycomb group proteins in maintaining bone marrow-derived mesenchymal stromal cells

The molecular mechanisms that maintain bone marrow-derived mesenchymal stromal cells in an undetermined state are not entirely understood. In our study, the maintenance of mesenchymal progenitor numbers was altered in *Cbx2*$^{cterm/cterm}$ mice. Recent reports have described the function of polycomb group genes in bone marrow-derived mesenchymal stromal cells maintenance. *Pcgf4/Bmi1*nullizygous mice and *Asxl*$^{fl/fl}$;*Osx-cre* mice clearly demonstrated a reduction in the number of bone marrow-derived mesenchymal stromal cells in mice at the weaning stage [44,52].

The role of polycomb group genes in maintaining in bone marrow-derived mesenchymal stromal cells may be shared. To manifest the underlying molecular mechanisms, further studies using mice in which individual polycomb group genes are ablated are required.

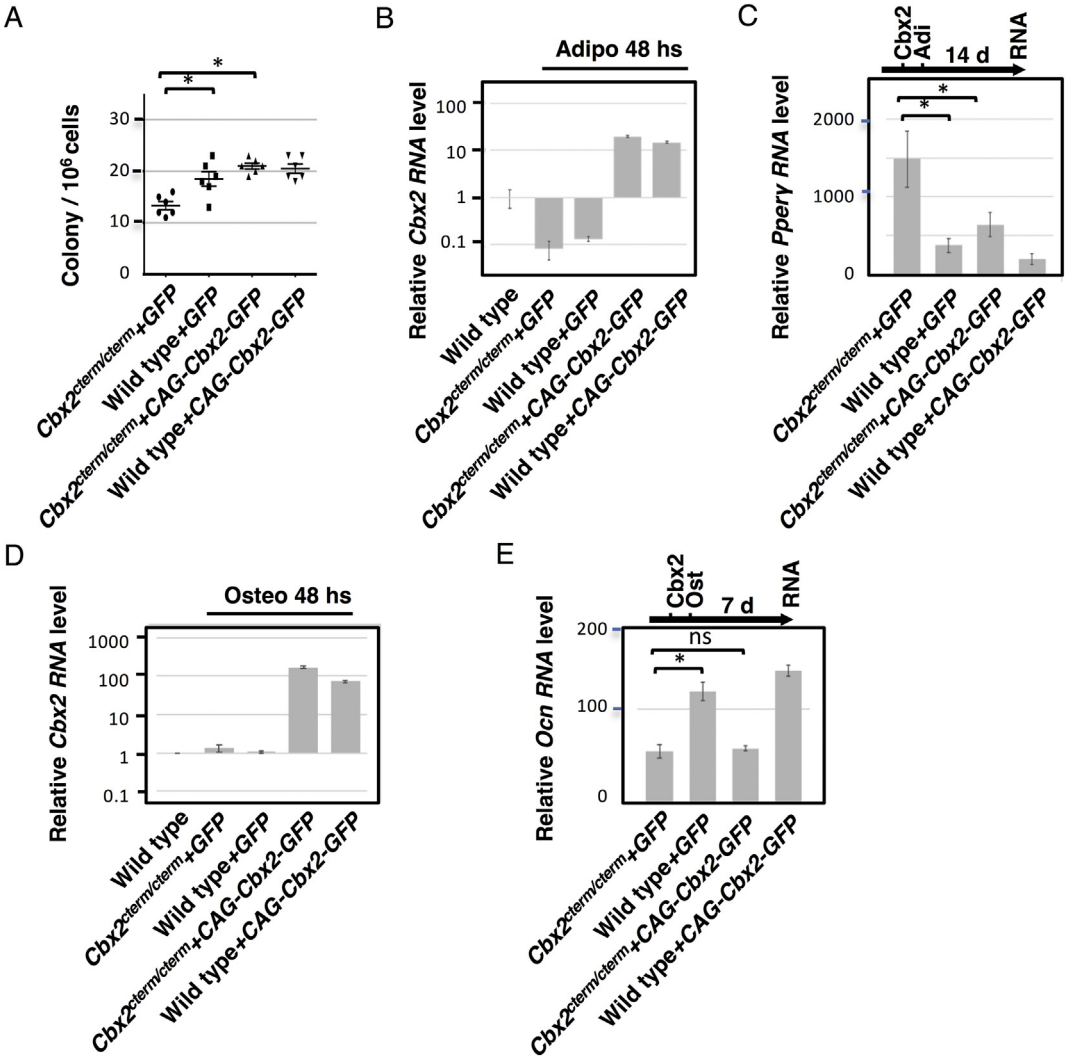

Fig. 8. (A) *Cbx2* was forced expressed by control *GFP* or *CAG-Cbx2-GFP* in primary bone marrow stroma cells from wild type (n = 3, XX = 3) or $Cbx2^{cterm/cterm}$ mice (n = 3, XX = 1, XY = 2), and only colony numbers of fibroblasts were counted. Numbers of colony per 10^6 cells are shown. Data are mean ± SD. *, $p < 0.05$. (A, C) (B) Passaged and pooled bone marrow stromal cells from wild type (n = 3, XY = 1, XX = 2) or $Cbx2^{cterm/cterm}$ mice (n = 3, XY = 1, XX = 2) were transfected with control *GFP* or *CAG-Cbx2-GFP*. After 48 h, RNA was extracted and used for *Cbx2* quantitation by real time PCR. Expression level of *Cbx2* in un-transfected wild type cells in normal medium is set as 1. Because $Cbx2^{cterm/cterm}$ mice were generated by Poly A capture type targeting vector [21], $Cbx2^{cterm/cterm}$ cells expressed as much *Cbx2* as wild type. (C) Three days after transfection, cells were cultured in a medium for adipogenic differentiation for 14 days at a density of 5×10^4 cells per well in 12-well-plates. RNA extracted from 3 wells for each genotype was quantitated by real time PCR. Relative levels of *Pparγ2* were measured. Data are mean ± SD. *, $p < 0.05$. Expression level of *Pparγ2* in undifferentiated wild type is set as 1. (D) Cbx2 rescue experiment in osteoblastic differentiation condition failed to rescue osteogenic gene expression. In these experiments, Cbx2 transfected *Cbx2*KO passaged and pooled stromal cells expressed almost the same levels of *Ocn* as *Cbx2*KO. (E) Three days after transfection, cells were cultured in a medium for osteoblastic differentiation for 7 days. RNA extracted from 3 wells for each genotype was quantitated by real time PCR. Relative levels of *Ocn* were measured. Data are mean ± SD. *, $p < 0.05$. ns, not significant. Expression level of *Ocn* in undifferentiated wild type is set as 1.

4.5. *Cbx2 functions in the adipocyte lineage and regulates Pparγ expression*

Our data indicate that Cbx2 is a negative regulator of adipocyte differentiation. Its loss accelerated adipocyte differentiation, while its forced expression suppressed adipocyte differentiation. In addition, our RT-qPCR analyses using bone marrow stromal cells and the genome-wide expression profile from another group using mouse bone narrow stromal cell line ST2 [60] suggested that Cbx2 is one of the epigenetic components protecting multipotent mesenchymal stromal cells. Considering the rapid downregulation of Cbx2 during adipogenic differentiation (Fig. 8B and [60]), we assumed that Cbx2 could protect the stromal cells from leaky adipogenic differentiation. Bivalent chromatin domains, which have both repressive H3K27me3 and active H3K4me3 features, were detected in *Pparγ* and *Cebpa* in embryonic stem cell and mouse embryonic fibroblasts [61], and in these genes, transcription is poised in the course of adipogenic differentiation [62]. Because Cbx2 preferentially binds to H3K27me3 [63], it is possible that Cbx2 functions to poise *Pparγ* and *Cebpa* activation. Cbx2-mediated inhibition of adipogenic lineage commitment during the maintenance of multipotent bone marrow mesenchymal stromal cells might occur both in vitro and in vivo. While in osteogenic genes, forced expressed Cbx2 could not rescue *Cbx2* deficient phenotype. These data presumably indicated the Cbx2 disrupted in vivo could be irreversible.

In summary, we demonstrate that *Cbx2* controls skeletal development and bone formation. Indeed, the growth plate and trabecular bone in the femur and tibia were hypoplastic in $Cbx2^{cterm/cterm}$ mice, as are head bones. Furthermore, the pool of mesenchymal progenitors diminished in these mice, with a clear bias toward expression of adipogenic genes. These results highlight the unique role of mouse polycomb *Cbx2* in adipogenic cell fates.

Conflict of interest

The authors declare no conflict of interest.

Acknowledgments

This study was supported by Grants-in-Aid from Japan Society for the Promotion of Science (15K06917) and by Takeda Foundation. The funding sources were not involved in the study design; in the collection, analysis, and interpretation of data; in the writing of the report; and in the decision to submit the article for publication.

Appendix A. Supplementary data

Supplementary data to this article can be found online at https://doi.org/10.1016/j.bone.2018.10.021.

References

[1] C. Lanzuolo, V. Orlando, Memories from the polycomb group proteins, Annu. Rev. Genet. 46 (2012) 561–589.
[2] J.A. Smon, R.E. Kingston, Mechanisms of polycomb gene silencing: knowns and unknowns, Nat. Rev. Mol. Cell Biol. 10 (2009) 697–708.
[3] J.A. Simon, R.E. Kingston, Occupying chromatin: polycomb mechanisms for getting to genomic targets, stopping transcriptional traffic, and staying put, Mol. Cell 49 (2013) 808–824.
[4] R. Paro, H. Strutt, G. Cavalli, Heritable chromatin states induced by the Polycomb and trithorax group genes, Novartis Found. Symp. 214 (1998) 51–61.
[5] Z. Shao, F. Raible, R. Mollaaghababa, J.R. Guyon, C.T. Wu, W. Bender, R.E. Kingston, Stabilization of chromatin structure by PRC1, a Polycomb complex, Cell 98 (1999) 37–46.
[6] A. Franke, M. DeCamillis, D. Zink, N. Cheng, H.W. Brock, R. Paro, Polycomb and polyhomeotic are constituents of a multimeric protein complex in chromatin of *Drosophila melanogaster*, EMBO J. 11 (1992) 2941–2950.
[7] R. Cao, Y. Zhang, The functions of E(Z)/EZH2-mediated methylation of lysine 27 in histone H3, Curr. Opin. Genet. Dev. 14 (2004) 155–164.
[8] Z. Gao, J. Zhang, R. Bonasio, F. Strino, A. Sawai, F. Parisi, Y. Kluger, D. Reinberg, PCGF homologs, CBX proteins, and RYBP define functionally distinct PRC1 family complexes, Mol. Cell 45 (2012) 344–356.
[9] G. Mas, L. Di Croce, The role of Polycomb in stem cell genome architecture, Curr. Opin. Cell Biol. 43 (2016) 87–95.
[10] D. O'Carroll, S. Erhardt, M. Pagani, S.C. Barton, M.A. Surani, T. Jenuwein, The polycomb-group gene Ezh2 is required for early mouse development, Mol. Cell. Biol. 21 (2001) 4330–4336.
[11] D. Pasini, A.P. Bracken, M.R. Jensen, E. Lazzerini Denchi, K. Helin, Suz12 is essential for mouse development and for EZH2 histone methyltransferase activity, EMBO J. 23 (2004) 4061–4071.
[12] C. Faust, A. Schumacher, B. Holdener, T. Magnuson, The eed mutation disrupts anterior mesoderm production in mice, Development 121 (1995) 273–285.
[13] M. Boulard, J.R. Edwards, T.H. Bestor, FBXL10 protects Polycomb-bound genes from hypermethylation, Nat. Genet. 47 (2015) 479–485.
[14] M.K. Pirity, J. Locker, N. Schreiber-Agus, Rybp/DEDAF is required for early post-implantation and for central nervous system development, Mol. Cell. Biol. 25 (2005) 7193–7202.
[15] J.W. Voncken, B.A.J. Roelen, M. Roefs, S. de Vries, E. Verhoeven, S. Marino, J. Deschamps, M. van Lohuizen, Rnf2 (Ring1b) deficiency causes gastrulation arrest and cell cycle inhibition, Proc. Natl. Acad. Sci. U. S. A. 100 (2003) 2468–2473.
[16] T. Akasaka, M. Kanno, R. Balling, M.A. Mieza, M. Taniguchi, H. Koseki, A role for mel-18, a Polycomb group-related vertebrate gene, during the anteroposterior specification of the axial skeleton, Development 122 (1996) 1513–1522.
[17] M.J. Alkema, N.M. van der Lugt, R.C. Bobeldijk, A. Berns, M. van Lohuizen, Transformation of axial skeleton due to overexpression of bmi-1 in transgenic mice, Nature 374 (1995) 724–727.
[18] N. Coré, S. Bel, S.J. Gaunt, M. Aurrand-Lions, J. Pearce, A. Fisher, M. Djabali, Altered cellular proliferation and mesoderm patterning in Polycomb-M33-deficient mice, Development 124 (1997) 721–729.
[19] M. del Mar Lorente, C. Marcos-Gutiérrez, C. Pérez, J. Schoorlemmer, A. Ramírez, T. Magin, M. Vidal, Loss- and gain-of-function mutations show a polycomb group function for Ring1A in mice, Development 127 (2000) 5093–5100.
[20] K. Isono, Y. Fujimura, J. Shinga, M. Yamaki, J. O-Wang, Y. Takihara, Y. Murahashi, Y. Takada, Y. Mizutani-Koseki, H. Koseki, Mammalian polyhomeotic homologues Phc2 and Phc1 act in synergy to mediate polycomb repression of Hox genes, Mol. Cell. Biol. 25 (2005) 6694–6706.
[21] Y. Katoh-Fukui, R. Tsuchiya, T. Shiroishi, Y. Nakahara, N. Hashimoto, K. Noguchi, T. Higashinakagawa, Male-to-female sex reversal in M33 mutant mice, Nature 393 (1998) 688–692.
[22] M. Suzuki, Y. Mizutani-Koseki, Y. Fujimura, H. Miyagishima, T. Kaneko, Y. Takada, T. Akasaka, H. Tanzawa, Y. Takihara, M. Nakano, H. Masumoto, M. Vidal, K. Isono, H. Koseki, Involvement of the Polycomb-group gene Ring1B in the specification of the anterior-posterior axis in mice, Development 129 (2002) 4171–4183.
[23] Y. Takihara, D. Tomotsune, M. Shirai, Y. Katoh-Fukui, K. Nishii, M.A. Motaleb, M. Nomura, R. Tsuchiya, Y. Fujita, Y. Shibata, T. Higashinakagawa, K. Shimada, Targeted disruption of the mouse homologue of the *Drosophila* polyhomeotic gene leads to altered anteroposterior patterning and neural crest defects, Development 1 (24) (1997) 3673–3682.
[24] N.M. van der Lugt, J. Domen, K. Linders, M. van Roon, E. Robanus-Maandag, H. te Riele, M. van der Valk, J. Deschamps, M. Sofroniew, M. van Lohuizen, A. Berns, Posterior transformation, neurological abnormalities, and severe hematopoietic defects in mice with a targeted deletion of the bmi-1 proto-oncogene, Genes Dev. 8 (1994) 757–769.
[25] A. Iwama, H. Oguro, M. Negishi, Y. Kato, Y. Morita, H. Tsukui, H. Ema, T. Kamijo, Y. Katoh-Fukui, H. Koseki, M. van Lohuizen, H. Nakauchi, Enhanced self-renewal of hematopoietic stem cells mediated by the polycomb gene product Bmi-1, Immunity 21 (2004) 843–851.
[26] H. Oguro, A. Iwama, Y. Morita, T. Kamijo, M. van Lohuizen, H. Nakauchi, Differential impact of Ink4a and Arf on hematopoietic stem cells and their bone marrow microenvironment in Bmi1-deficient mice, J. Exp. Med. 203 (2006) 2247–2253.
[27] H. Ohta, A. Sawada, J.Y. Kim, S. Tokimasa, S. Nishiguchi, R.K. Humphries, J. Hara, Y. Takihara, Polycomb group gene rae28 is required for sustaining activity of hematopoietic stem cells, J. Exp. Med. 195 (2002) 759–770.
[28] I.K. Park, D. Qian, M. Kiel, M.W. Becker, M. Pihalja, I.L. Weissman, S.J. Morrison, M.F. Clarke, Bmi-1 is required for maintenance of adult self-renewing haematopoietic stem cells, Nature 423 (2003) 302–305.
[29] M. Vidal, K. Starowicz, Polycomb complexes PRC1 and their function in hematopoiesis, Exp. Hematol. 48 (2017) 12–31.
[30] M. Shirai, T. Osugi, H. Koga, Y. Kaji, E. Takimoto, I. Komuro, J. Hara, T. Miwa, K. Yamauchi-Takihara, Y. Takihara, The Polycomb-group gene Rae28 sustains Nkx2.5/Csx expression and is essential for cardiac morphogenesis, J. Clin. Invest. 110 (2002) 177–184.
[31] Y. Katoh-Fukui, K. Miyabayashi, T. Komatsu, A. Owaki, T. Baba, Y. Shima, T. Kidokoro, Y. Kanai, A. Schedl, D. Wilhelm, P. Koopman, Y. Okuno, K. Morohashi, Cbx2, a polycomb group gene, is required for Sry gene expression in mice, Endocrinology 153 (2012) 913–924.
[32] Y. Katoh-Fukui, A. Owaki, Y. Toyama, M. Kusaka, Y. Shinohara, M. Maekawa, K. Toshimori, K. Morohashi, Mouse Polycomb M33 is required for splenic vascular and adrenal gland formation through regulating Ad4BP/SF1 expression, Blood 106 (2005) 1612–1620.
[33] L.A. Boyer, K. Plath, J. Zeitlinger, T. Brambrink, L.A. Medeiros, T.I. Lee, S.S. Levine, M. Wernig, A. Tajonar, M.K. Ray, G.W. Bell, A.P. Otte, M. Vidal, D.K. Gifford, R.A. Young, R. Jaenisch, Polycomb complexes repress developmental regulators in murine embryonic stem cells, Nature 441 (2006) 349–353.
[34] F. Mohn, M. Weber, M. Rebhan, T.C. Roloff, J. Richter, M.B. Stadler, M. Bibel, D. Schübeler, Lineage-specific polycomb targets and de novo DNA methylation define restriction and potential of neuronal progenitors, Mol. Cell 30 (2008) 755–766.
[35] C. Colnot, C. Lu, D. Hu, J.A. Helms, Distinguishing the contributions of the perichondrium, cartilage, and vascular endothelium to skeletal development, Dev. Biol. 269 (2004) 55–69.
[36] C. Maes, T. Kobayashi, M.K. Selig, S. Torrekens, S.I. Roth, S. Mackem, G. Carmeliet, H.M. Kronenberg, Osteoblast precursors, but not mature osteoblasts, move into developing and fractured bones along with invading blood vessels, Dev. Cell 19 (2010) 329–344.
[37] L. Yang, K.Y. Tsang, H.C. Tang, D. Chan, K.S. Cheah, Hypertrophic chondrocytes can become osteoblasts and osteocytes in endochondral bone formation, PNAS 111 (2014) 12097–12102.
[38] T. Komori, H. Yagi, S. Nomura, A. Yamaguchi, K. Sasaki, K. Deguchi, Y. Shimizu, R.T. Bronson, Y.H. Gao, M. Inada, M. Sato, R. Okamoto, Y. Kitamura, S. Yoshiki, T. Kishimoto, Targeted disruption of Cbfa1 results in a complete lack of bone formation owing to maturational arrest of osteoblasts, Cell 89 (1997) 755–764.
[39] A.G. Cristancho, M.A. Lazar, Forming functional fat: a growing understanding of adipocyte differentiation, Nat. Rev. Mol. Cell Biol. 12 (2011) 722–734.
[40] S.R. Farmer, Transcriptional control of adipocyte formation, Cell Metab. 4 (2006) 263–273.
[41] E.L. Scheller, W.P. Cawthorn, A.A. Burr, M.C. Horowitz, O.A. MacDougald, Marrow adipose tissue: trimming the fat, Trends Endocrinol. Metab. 27 (2016) 392–403.
[42] M.I. Lefterova, A.K. Haakonsson, M.A. Lazar, S. Mandrup, PPARγ and the global map of adipogenesis and beyond, Trends Endocrinol. Metab. 25 (2014) 293–302.
[43] L. Ye, Z. Fan, B. Yu, J. Chang, K. Al Hezaimi, X. Zhou, N.H. Park, C.Y. Wang, Histone demethylases KDM4B and KDM6B promotes osteogenic differentiation of human MSCs, Cell Stem Cell 11 (2012) 50–61.
[44] P. Zhang, C. Xing, S.D. Rhodes, Y. He, K. Deng, Z. Li, F. He, C. Zhu, L. Nguyen, Y. Zhou, S. Chen, K.S. Mohammad, T.A. Guise, O. Abdel-Wahab, M. Xu, Q.F. Wang, F.C. Yang, Loss of Asxl1 alters self-renewal and cell fate of bone marrow stromal cell, leading to Bohring-Opitz-like syndrome in mice, Stem Cell Rep. 6 (2016) 914–925.
[45] S. Hemming, D. Cakouros, S. Isenmann, L. Cooper, D. Menicanin, A. Zannettino, S. Gronthos, EZH2 and KDM6A act as an epigenetic switch to regulate mesenchymal stem cell lineage specification, Stem Cells 32 (2014) 802–815.
[46] A. Nagy, M. Gertsenstein, K. Vintersten, R. Behringer, Manipulating the Mouse Embryo: A Laboratory Manual, 3rd ed., Cold Spring Harbor Laboratory Press, New York, 2003.
[47] S. Andrews, FastQC: A Quality Control Tool for High Throughput Sequence Data, http://www.bioinformatics.babraham.ac.uk/projects/fastqc, (2015) Version 0.11.4.
[48] D. Kim, G. Pertea, C. Trapnell, H. Pimentel, R. Kelley, S.L. Salzberg, TopHat2:

accurate alignment of transcriptomes in the presence of insertions, deletions and gene fusions, Genome Biol. 14 (2013) R36.
[49] C. Trapnell, D.G. Hendrickson, M. Sauvageau, L. Goff, J.L. Rinn, L. Pachter, Differential analysis of gene regulation at transcript resolution with RNA-seq, Nat. Biotechnol. 31 (2013) 46–53.
[50] G. Dennis Jr., B.T. Sherman, D.A. Hosack, J. Yang, W. Gao, H.C. Lane, R.A. Lempicki, DAVID: database for annotation, visualization, and integrated discovery, Genome Biol. 4 (2003) R60.
[51] D.W. Huang, B.T. Sherman, R.A. Lempicki, Systematic and integrative analysis of large gene lists using DAVID bioinformatics resources, Nat. Protoc. 4 (2009) 44–57.
[52] H.W. Zhang, J. Ding, J.L. Jin, J. Guo, J.N. Liu, A. Karaplis, D. Goltzman, D. Miao, Defects in mesenchymal stem cell self-renewal and cell fate determination lead to an osteopenic phenotype in Bmi-1 null mice, J. Bone Miner. Res. 25 (2010) 640–652.
[53] A. Dudakovic, E.T. Camilleri, S.M. Riester, C.R. Paradise, M. Gluscevic, T.M. O'Toole, R. Thaler, J.M. Evans, H. Yan, M. Subramaniam, J.R. Hawse, G.S. Stein, M.A. Montecino, M.E. McGee-Lawrence, J.J. Westendorf, A.J. van Wijnen, Enhancer of zeste homolog 2 inhibition stimulates bone formation and mitigates bone loss caused by ovariectomy in skeletally mature mice, J. Biol. Chem. 291 (2016) 24594–24606.
[54] D. Schwarz, S. Varum, M. Zemke, A. Schöler, A. Baggiolini, K. Draganova, H. Koseki, D. Schübeler, L. Sommer, Ezh2 is required for neural crest-derived cartilage and bone formation, Development 141 (2014) 867–877.
[55] Z. Liu, T. Han, S. Fishman, J. Butler, T. Zimmermann, F. Tremblay, C. Harbison, N. Agrawal, J.J. Kopchick, M.B. Schaffler, S. Yakar, Ablation of hepatic production of the acid-labile subunit in bovine-GH transgenic mice: effects on organ and skeletal growth, Endocrinology 158 (2017) 2556–2571.
[56] S. Maezawa, K. Hasegawa, M. Yukawa, A. Sakashita, K.G. Alavattam, P.R. Andreassen, M. Vidal, H. Koseki, A. Barski, S.H. Namekawa, Polycomb directs timely activation of germline genes in spermatogenesis, Genes Dev. 31 (2017) 1693–1703. Aug.
[57] T. Kondo, K. Isono, K. Kondo, T.A. Endo, S. Itohara, M. Vidal, H. Koseki, Polycomb potentiates meis2 activation in midbrain by mediating interaction of the promoter with a tissue-specific enhancer, Dev. Cell 28 (2014) 94–101.
[58] X. Zhou, X. Dai, X. Wu, J. Ji, A. Karaplis, D. Goltzman, X. Yang, D. Miao, Overexpression of Bmi1 in lymphocytes stimulates skeletogenesis by improving the osteogenic microenvironment, Sci. Rep. 6 (2016) 29171.
[59] A. Greenbaum, Y.M. Hsu, R.B. Day, L.G. Schuettpelz, M.J. Christopher, J.N. Borgerding, T. Nagasawa, D.C. Link, CXCL12 in early mesenchymal progenitors is required for haematopoietic stem-cell maintenance, Nature 495 (2013) 227–230.
[60] Y. Tokuzawa, K. Yagi, Y. Yamashita, Y. Nakachi, I. Nikaido, H. Bono, Y. Ninomiya, Y. Kanesaki-Yatsuka, M. Akita, H. Motegi, S. Wakana, T. Noda, F. Sablitzky, S. Arai, R. Kurokawa, T. Fukuda, T. Katagiri, C. Schönbach, T. Suda, Y. Mizuno, Y. Okazaki, Id4, a new candidate gene for senile osteoporosis, acts as a molecular switch promoting osteoblast differentiation, PLoS Genet. 6 (2010) e1001019.
[61] T.S. Mikkelsen, Z. Xu, X. Zhang, L. Wang, J.M. Gimble, E.S. Lander, E.D. Rosen, Comparative epigenomic analysis of murine and human adipogenesis, Cell 143 (2010) 156–169.
[62] Y. Matsumura, R. Nakaki, T. Inagaki, A. Yoshida, Y. Kano, H. Kimura, T. Tanaka, S. Tsutsumi, M. Nakao, T. Doi, K. Fukami, T.F. Osborne, T. Kodama, H. Aburatani, J. Sakai, H3K4/H3K9me3 bivalent chromatin domains targeted by lineage-specific DNA methylation pauses adipocyte differentiation, Mol. Cell 60 (2015) 584–596.
[63] E. Bernstein, E.M. Duncan, O. Masui, J. Gil, E. Heard, C.D. Allis, Mouse polycomb proteins bind differentially to methylated histone H3 and RNA and are enriched in facultative heterochromatin, Mol. Cell. Biol. 26 (2006) 2560–2569.